REVIEW OF SCIENTIFIC INSTRUMENTS **86**, 113506 (2015)

Technique for fabrication of ultrathin foils in cylindrical geometry for liner-plasma implosion experiments with sub-megaampere currents

D. A. Yager-Elorriaga,[a] A. M. Steiner, S. G. Patel, N. M. Jordan, Y. Y. Lau, and R. M. Gilgenbach
Department of Nuclear Engineering and Radiological Sciences, University of Michigan, Ann Arbor, Michigan 48109-2104, USA

(Received 24 July 2015; accepted 3 November 2015; published online 19 November 2015)

In this work, we describe a technique for fabricating ultrathin foils in cylindrical geometry for liner-plasma implosion experiments using sub-MA currents. Liners are formed by wrapping a 400 nm, rectangular strip of aluminum foil around a dumbbell-shaped support structure with a non-conducting center rod, so that the liner dimensions are 1 cm in height, 6.55 mm in diameter, and 400 nm in thickness. The liner-plasmas are imploded by discharging ~600 kA with ~200 ns rise time using a 1 MA linear transformer driver, and the resulting implosions are imaged four times per shot using laser-shadowgraphy at 532 nm. This technique enables the study of plasma implosion physics, including the magneto Rayleigh-Taylor, sausage, and kink instabilities on initially solid, imploding metallic liners with university-scale pulsed power machines. © *2015 AIP Publishing LLC.* [http://dx.doi.org/10.1063/1.4935838]

I. INTRODUCTION

Recent experimental investigations of the Magnetized Liner Inertial Fusion (MagLIF) concept[1–4] have shown that it is possible to obtain temperatures as high as 3 keV and deuterium-deuterium fusion yields in excess of 10^{12} neutrons by compressing a preheated, magnetized fusion fuel inside a cylindrical liner driven by a multi-megaampere current on the 25 MA Z facility at Sandia National Laboratories.[4] One of the limitations to optimal compression in MagLIF experiments is the development of instabilities in the imploding liner. In particular, the magneto-Rayleigh-Taylor (MRT) instability, which occurs when a light material (magnetic field) accelerates a heavy material (plasma), develops on the outer surface of the liner during the implosion[5] and may feed-through to the inner liner surface and fuel,[6] limiting fuel confinement and achievable pressure.

Experiments studying the physics of Z-pinch plasmas and relevant plasma instabilities are commonly performed on university-scale pulsed power machines with peak current capabilities in the megaampere range.[7–10] These facilities have the advantages of relatively low cost per shot and high repetition rate compared to large-scale experiments such as Z, allowing for increased flexibility in designing and performing physics experiments. However, metallic liner-plasma implosions are difficult to study on small-scale experiments because the maximum attainable current is often insufficient to implode initially solid liners of reasonable geometry. These experiments typically focus on imploding wire arrays or the physics of non-imploding liners, such as the initiation of plasma and instabilities on the surface or the precursor plasma formed inside of the liner.[11–14]

To achieve an implosion with a relatively low current, a small liner radius and a low linear mass (mass per length) are required. If the radius is too small, the distance over which the liner can implode becomes prohibitively short, so in practice, an extremely thin liner is needed to achieve an implosion on a sub-MA machine. For example, previous experiments in the megaampere regime used 6 μm thick, 3 mm diameter aluminum liners to achieve implosions using peak currents of ~1.2 MA.[15] Experiments with sub-MA currents require much thinner liners since the driving magnetic pressure for a Z-pinch scales with load current squared. The required thickness may be estimated using a simple 0-D force model (described in Section IV) where the dynamics of a thin shell are calculated using the magnetic pressure generated from the current pulse. This model shows that for a 550 kA current pulse with 220 ns base-to-peak rise time, a 6 mm diameter liner requires a thickness of 400 nm to implode by peak current. A liner of this thickness cannot maintain its own form and requires a support structure that does not significantly impede the implosion.

In this work, we develop and implement a method for fabricating 400 nm thick, 6.55 mm diameter liner targets using a dumbbell-shaped support structure for use on the linear transformer driver (LTD) facility at the University of Michigan. Successful implosions of these liners are demonstrated using drive currents of ~600 kA with rise times of ~200 ns. For this current, the magnetic pressure that drives the implosion is only 36% of that generated in a megaampere discharge, showing that it is possible to dramatically reduce the current and magnetic pressure requirements to achieve an implosion. Characteristic plasma instabilities are observed during the implosions, including the electrothermal (ET),[16] MRT,[5,7] and sausage instabilities. This liner fabrication method allows sub-MA pulsed power machines to study the plasma physics phenomena unique to imploding

[a]Electronic mail: dyager@umich.edu

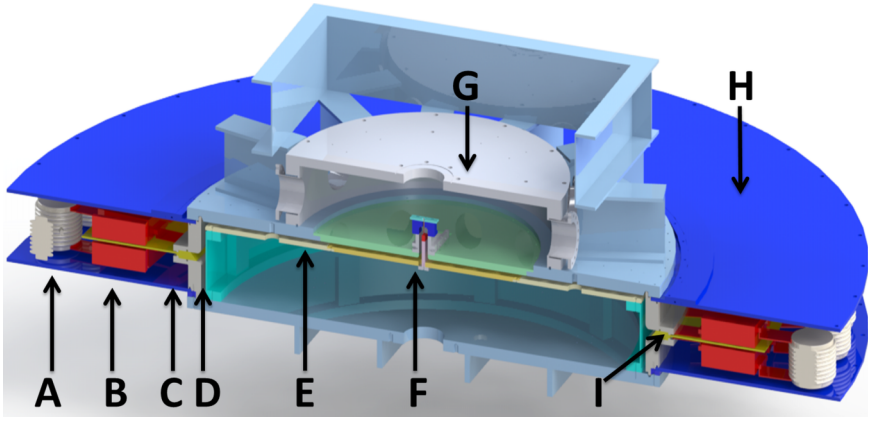

FIG. 1. Cutout of the LTD and transmission line. (A) Spark gap switch, (B) capacitor, (C) iron core section, (D) coaxial transmission line, (E) radial transmission line, (F) load hardware with a triplate transmission line, (G) vacuum chamber, (H) oil chamber, and (I) insulator.

plasmas and compare results with contemporary theoretical investigations.[6,17,18]

II. EXPERIMENTAL CONFIGURATION AND DIAGNOSTICS

The pulsed power driver used in these experiments is the Michigan Accelerator for Inductive Z-Pinch Experiments (MAIZE) LTD,[7,10] which is capable of delivering 1 MA of current into a matched load at ±100 kV charge.[19,20] For these liner-plasma implosion experiments, the power from the driver is delivered to the load using a coaxial-to-radial-to-triplate transmission line (Fig. 1). The triplate cathode is connected to the liner, and the return current is split via the two outer anode plates (Fig. 2), allowing access for laser imaging. The triplate transmission line and load hardware are located in a 1-m-diameter vacuum chamber. When the chamber is placed under vacuum, atmospheric pressure compresses the anode-cathode (AK) gap of the transmission line by 1.2 mm, presenting a challenge for load hardware design. The inductance from the transmission line and generator (~13 nH) and liner load (~15 nH) results in a peak current of 600 kA for ±70 kV capacitor charging voltage.

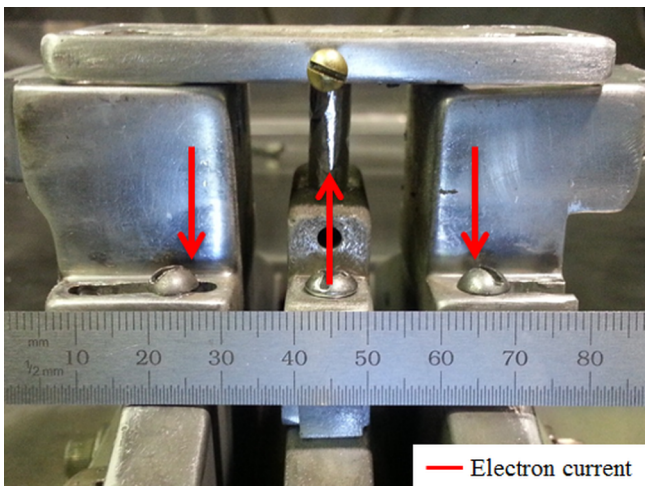

FIG. 2. Liner load (center) and current path. Arrows show the direction of electron flow.

The diagnostics used include B-dot current monitors and a 2 ns pulse length, frequency-doubled Nd:YAG laser for shadowgraphy at 532 nm. The beam is split into four paths/delays to image the plasma at 20 ns intervals. The beams intersect the load on the same horizontal plane at 1.3° ± 0.2° intervals, giving a total angular spread of the four beams of 3.9°. The shadowgraphs are captured using Canon Rebel XTi and XSi cameras. The resolutions for all beam paths are measured at better than 100 μm/line pair using a 1951 USAF resolution target. A 2.36 mm thick plastic shield is placed between the load and vacuum window ports to protect the windows from load debris. Neutral density filters and 532 nm line filters are used to limit plasma self-emission on the shadowgraph images.

III. LINER FABRICATION

Fabrication techniques for ultrathin-walled liners require a support structure that does not significantly impede the implosion. The liners are constructed using 400 nm thick, rectangular strips of aluminum foil (99.1% pure, obtained from Goodfellow[21]) wrapped around a dumbbell-shaped support structure as shown in Fig. 3. The surface of the foil was characterized using an atomic force microscope (AFM) and shows ~300 nm tall bumps and pits extending over ~30 μm, as shown in Fig. 4. These imperfections persisted even when applying tension to the foil and are therefore inherent to the liner surface. As we shall see, it is these small scale imperfections that dominate the initial stage of the implosion and seed the subsequent evolution of the instabilities observed.

The support structure is fabricated from a ~3 cm long, 1/4 in. (6.35 mm) diameter plastic rod made of nylon 6/6. A 1 cm long section of the plastic rod, referred to as the liner region in Fig. 3(a), is reduced to a diameter of between 1 and 2 mm using a tabletop lathe. Aluminum tape (0.1 mm thickness) is wrapped around the ends of the structure, referred to as the support regions. The aluminum foil is then cut to a rectangular strip with dimensions 1.5 cm by 2.2 cm and carefully wrapped around the liner region so that the foil contacts the aluminum tape on both ends. The rectangular strip is cut slightly longer than the circumference of the support structure to ensure that there is an overlapping region and not a gap. At this point

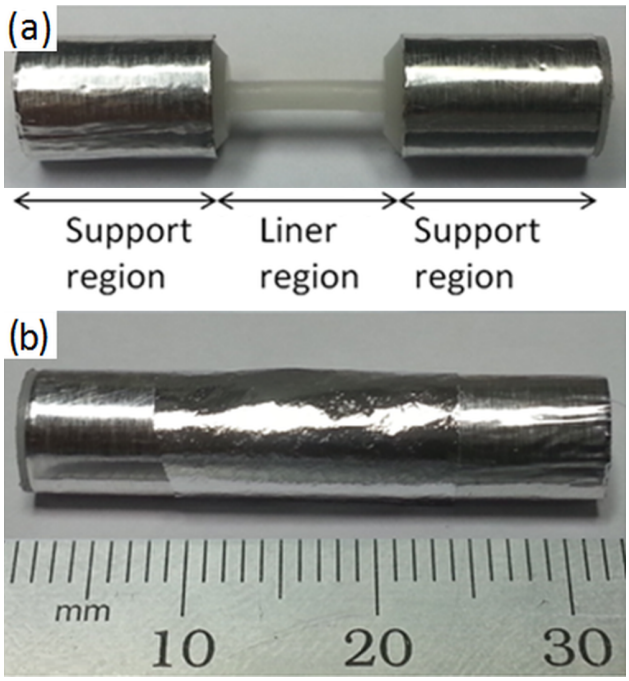

FIG. 3. (a) Liner support structure. (b) Assembled liner.

wrinkles in the foil are smoothed by carefully adjusting the position where the foil contacts the support structure. The thin foil naturally forms electrical contact by electrostatically adhering to the metallic support structure. The assembled liner is then loaded into the pulsed power machine so that the aluminum tape on the support regions makes electrical contact with the anode and cathode, as shown in Fig. 2. For this hardware, the anode and cathode have ~7 mm diameter holes machined so that the assembled liner and support structure can slide inside the electrodes. This is particularly useful in addressing the AK gap compression that occurs when the chamber is placed under vacuum. By fixing the liner load to the cathode or anode with a set screw, the unfixed end is able to slide into the opposing electrode. The electrical contact resistance using this sliding scheme has not been found to limit the current delivered to the load, as seen by comparing the measured current to the PSpice circuit simulation for the LTD generator[19] using the liner load inductance with negligible resistance, shown in Fig. 5.

Extreme care must be taken when handling the foils. In order to cut rectangular strips of foil, we found it useful to place the stock foil between two pieces of optical cleaning tissue. The foil and tissue are then placed on the top of a plastic surface and cut with a sharpened razor blade, using a straight edge as a guide. The top layer of tissue paper is then removed, leaving behind the cut aluminum foil. In general, it was helpful to handle the foil using rounded tweezers with the tips bent outward (the foil would tear if handled with the points of tweezers), and to smooth any wrinkles in the assembled liner by adjusting the contact of the foil to the support structure using the rounded edge of a dental pick.

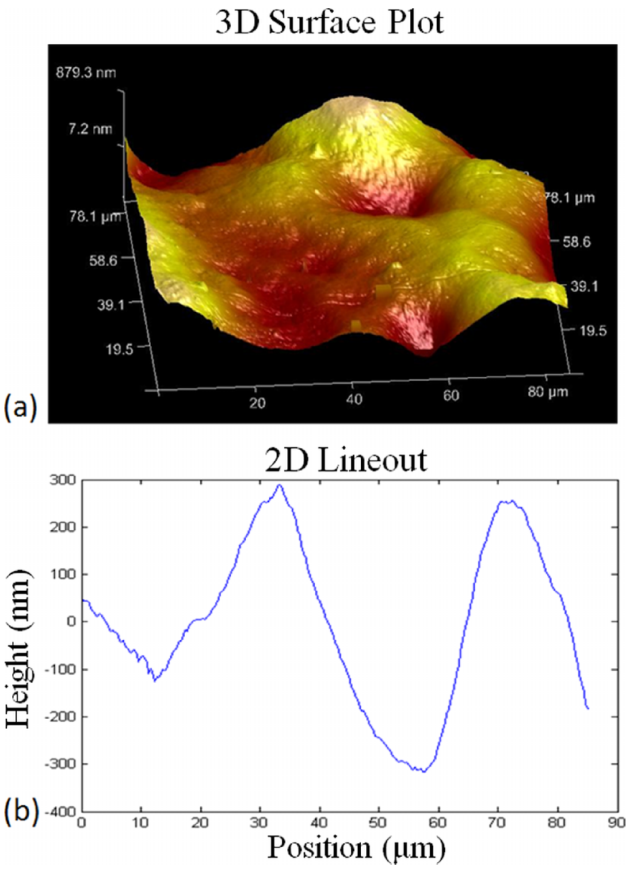

FIG. 4. (a) AFM surface plot of 400 nm foil. (b) 2D lineout highlighting changes in the surface topology.

IV. EXPERIMENTAL RESULTS

Current data from the linear transformer driver and timings for shadowgraphs are shown in Fig. 5. The peak current is fairly consistent at 600 kA with 220 ns rise time and agrees with the circuit modeling of the LTD and transmission line. A characteristic load inductance may be estimated from the current pulse by assuming a constant inductance and is found to be approximately 15 nH, agreeing with calculations using Ansys Maxwell. Shadowgraphs from three shots are depicted in Fig. 6 and include the outline of the initial position of the liner (dashed line) determined using a pre-shot image. The shadowgraphs are contrast enhanced and the plasma boundary is traced (solid line) using a boundary tracing algorithm. In

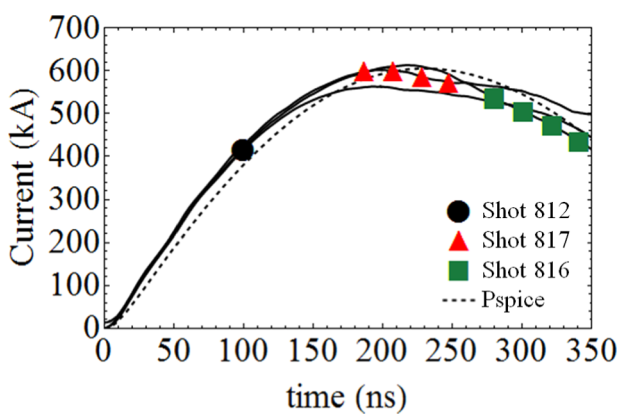

FIG. 5. LTD current traces and shadowgraph timings for shots 812, 817, and 816. The PSpice simulated current trace is also plotted (dashed line).

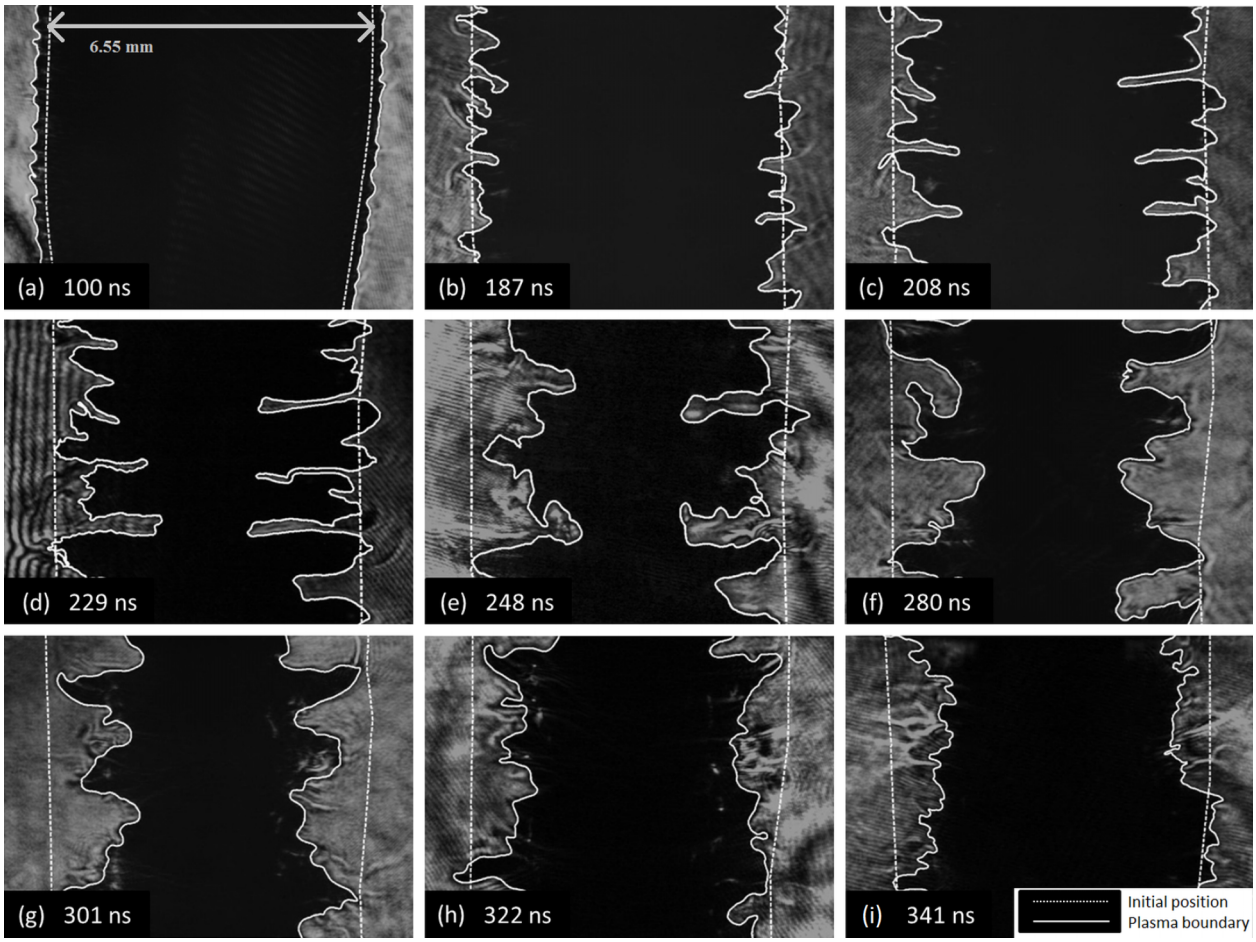

FIG. 6. Boundary-traced shadowgraphs (aspect ratio 1:1) for shots 812 (a), 817 (b)-(e), and 816 (f)-(i), showing the four stages of plasma dynamics that occur during the discharge: expansion (a), implosion (b)-(d), stagnation (e) and (f), and re-expansion (g)-(i).

order to use the boundary tracing algorithm, dark areas due to beam nonuniformities, diffraction patterns, and interference fringes are manually voided as needed, and a local spatial averaging algorithm is applied to smooth out the plasma-vacuum boundary. This allows bulk plasma features to be traced while avoiding tracing spurious features such as interference fringes or beam nonuniformities. The interference fringes on the left side of Fig. 6(d) are due to a shearing interferometer set up for this shot on this beam path.[22]

The radius of the observable plasma is determined using the boundary tracing algorithm and is shown in Fig. 7 for 13 shadowgraphs obtained from four shots. The average plasma radius R_{avg} is determined by averaging the radial extent of the plasma as a function of position over the region shown in Fig. 7(a). The maximum plasma radius is determined for the left and right sides of the plasma and averaged to obtain the characteristic maximum radius R_{max}. A similar method is used to determine the characteristic minimum radius R_{min}. These results are compared to a 0-D implosion model which assumes the mass of the liner is located at a single radius and calculates the trajectory from the $J \times B$ force for a current pulse $I(t)$, according to the equation

$$\frac{\hat{m}}{2\pi r(t)}\ddot{r}(t) = -\frac{B(t)^2}{2\mu} = -\frac{\mu I(t)^2}{8\pi^2 r(t)^2}, \quad (1)$$

where $\hat{m}$ is the liner mass per unit length, r and $\ddot{r}$ are the radius and second time-derivative of the radius, μ is the magnetic permeability, and $B(t)$ is the magnetic field generated by the current flowing in the liner.

V. ANALYSIS AND DISCUSSION

The shadowgraphs in Fig. 6 show that it is possible to implode an initially solid metal plasma with 600 kA current using the technique presented in this paper. This enables a variety of physics experiments to be performed, especially those relevant to instabilities and plasma dynamics observed in MagLIF implosions. The accessibility of the method allows extensive study of implosion instabilities in addition to the testing of mitigation techniques on university machines at a much lower cost than on large pulsed power machines such as the Z Machine.

As seen in the AFM data (Fig. 4), the foil surface is dominated by peaks and valleys ~300 nm in height and ~30 μm in width that provide the seed for early time instability growth. As the magnetic pressure ramps up, the MRT instability is seeded by these early time instability structures. This may be seen in the shadowgraphs in Figs. 6(a) and 6(b), which show the instabilities developing on the surface of the liner, including on the wrinkles and imperfections. Up to this point, the wave-

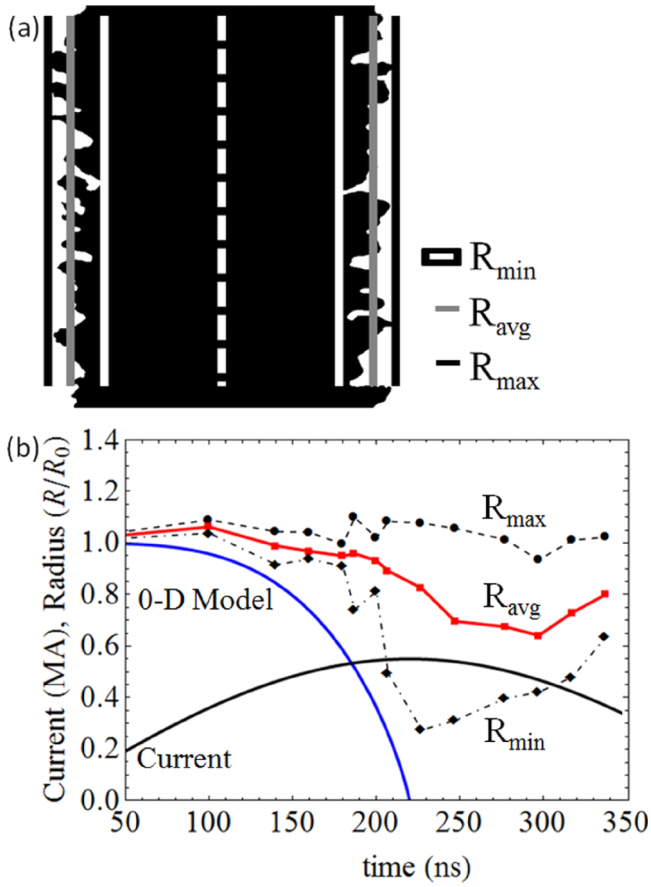

FIG. 7. (a) Definition of radii obtained from shadowgraphs plotted in part (b), where R_{avg} is the plasma radius averaged over liner length, and R_{max} and R_{min} are the average of the left and right maximum and minimum radii, respectively. (b) Comparison of radii to the 0-D implosion model using a typical current trace. All radii are normalized to the initial liner radius.

length of the instability structures is much smaller than the liner circumference—this means that the initial instabilities are effectively growing in planar geometry.[18] Thus, while the initial liner surfaces in Fig. 6 lack up-down symmetry and are not perfectly cylindrical, these latter irregularities are of a large enough spatial scale (millimeter-scale) that they are unimportant to the development of the small scale perturbations that were observed. Likewise, the inherent overlapping region (~7% of the total liner circumference) provides a seed to the very long wavelength m = 1 mode, which is similarly unimportant to the short wavelength perturbations observed during the implosion process. Nevertheless, all of these factors affect the azimuthal correlation for the longer wavelength MRT, despite the overall cylindrical symmetry. For example, the bottom of the shadowgraphs in Figs. 6(b)-6(d) show a longer wavelength, azimuthally correlated structure whereas the top does not—this may be due to a random lack of correlation in the initial "planar geometry" seed. Even a perfectly formed liner may develop nonuniformities as the AK gap compresses when the chamber is placed under vacuum, so we expect that the observed instabilities would follow a similar, but not identical, initiation and development. Therefore, such imperfect liners are still useful for studying instability structures, particularly with multiple shadowgraphy frames in a single shot.

The plasma dynamics may be interpreted in four stages: expansion (Fig. 6(a)), implosion (Figs. 6(b)-6(d)), stagnation (Figs. 6(e) and 6(f)), and re-expansion (Figs. 6(g)-6(i)). During the first stage, the solid-state aluminum is unstable to the striation form of ET, which causes regions of the liner to heat faster than the bulk material. These regions are the first to ablate and couple into longer wavelength structures that seed the subsequent MRT, an effect which has been observed in both Hydra simulations of liners[23] and experiments conducted at Sandia National Laboratories.[16] The shadowgraph at 100 ns (Fig. 6(a)) shows small wavelength structures of 0.3-0.6 mm, characteristic of early time instabilities of electrothermal origin observed on the same 400 nm foils in planar geometry.[7] In the second stage (Figs. 6(b)-6(d)), the magnetic pressure becomes large enough to drive the implosion so that the liner-plasma accelerates inward and is unstable to MRT and sausage modes (and to kink instabilities if an axial magnetic field is present[24]). Longer wavelength structures develop in the range of 0.5-1.5 mm, comparable to wavelengths observed in MRT experiments using 400 nm foils in planar geometry.[7] In the third stage (Figs. 6(g)-6(i)), the plasma has stagnated on the rod and is no longer accelerating inward so that the plasma is MRT stable but remains unstable to sausage modes.[18] Longer, azimuthally correlated instability structures form with wavelengths ranging from 1.7 to 3.0 mm. At around 300 ns (Fig. 6(g)), the final re-expansion stage begins as the magnetic pressure drops due to the decreasing current.

Comparison to the 0-D implosion model shows that the maximum and average plasma radii (R_{max} and R_{avg}) implode slower than the model predicts, while the minimum plasma boundary (R_{min}) shows a much better agreement. To interpret these results, one must keep in mind the limitations of the 532 nm laser backlighter, which is sensitive to mass trailing the implosion.[8] For example, the shadowgraph in Fig. 6(d) was taken around the 0-D predicted implosion time (220 ns) and shows a striking resemblance to a fully imploded Al wire array reported in Ref. 25: both show necks where the plasma approaches the axis as well as plasma that remains at the initial radii. The complete implosion dynamics may be better understood using x-ray radiography to fully probe the plasma; we leave this for future work.

Finally, a distinction must be made between ultrathin liners and MagLIF liners when considering skin depth effects. For the current rise time and aluminum liners used in this experiment, the initial skin depth (~75 μm) is much larger than the 0.4 μm liner thickness, whereas for a MagLIF beryllium liner the skin depth (~60 μm) is only a fraction of the ~500 μm liner thickness. This means that ultrathin liners are uniformly heated and ablated, whereas plasma on MagLIF liners is initiated on the outer liner surface only. Electrothermal instabilities, forming early in time while the liner is still solid, are consequently not directly comparable. When considering magneto hydrodynamic (MHD) plasma instabilities, however, the geometries have become much more comparable by the time the ultrathin liner implodes. At 100 ns, the outer surface has expanded about 200 μm outward against a large magnetic pressure, as seen in Fig. 6(a). To set a lower bound on thickness, let us assume that the plasma also expands inward 200 μm (against a small magnetic pressure) so that the plasma

thickness is estimated to be greater than 400 μm. The situation then becomes comparable to MagLIF where the lower density, ablated plasma on the liner surface is susceptible to MHD instabilities including MRT, sausage, and kink modes. For ultrathin liners, the imploding plasma column is susceptible to the same MHD instabilities. This means that the development and mitigation of these instabilities are especially relevant. In particular, by incorporating an axial magnetic field, the study of kink modes on ultrathin liners may shed insight into the helical modes observed in Ref. 24, which may be of MHD origin.

VI. CONCLUSION

We have presented a simple method for studying implosions of liner-plasmas in cylindrical geometry on sub-MA machines. While the plastic rod limits a full on-axis implosion, the technique described here enables a variety of physics to be investigated, including the seeding of MRT from ET, the stabilization of MRT using axial magnetic fields and magnetic shear, and the coupling of sausage and kink modes to MRT. Future experiments may achieve implosions with even smaller currents by using thinner foils or smaller initial radii; for example, following a 0-D implosion model, a 400 nm thick, 3 mm diameter Al liner may be imploded with ~210 kA with 200 ns base-to-peak rise time.

ACKNOWLEDGMENTS

This work was supported by the U.S. Department of Energy through Award No. DE-SC0012328. S.G. Patel and A.M. Steiner were supported by NPSC funded by Sandia. D.A. Yager-Elorriaga was supported by NSF fellowship Grant No. DGE 1256260. The authors would like to thank Dr. Matt Gomez of Sandia National Laboratories for creative discussions on liner fabrication techniques and offering helpful advice along the way.

[1]M. E. Cuneo, M. C. Herrmann, D. B. Sinars, S. A. Slutz, W. A. Stygar, R. A. Vesey, A. B. Sefkow, G. A. Rochau, G. A. Chandler, J. E. Bailey, J. L. Porter, R. D. McBride, D. C. Rovang, M. G. Mazarakis, E. P. Yu, D. C. Lamppa, K. J. Peterson, C. Nakhleh, S. B. Hansen, A. J. Lopez, M. E. Savage, C. A. Jennings, M. R. Martin, R. W. Lemke, B. W. Atherton, I. C. Smith, P. K. Rambo, M. Jones, M. R. Lopez, P. J. Christenson, M. A. Sweeney, B. Jones, L. A. McPherson, E. Harding, M. R. Gomez, P. F. Knapp, T. J. Awe, R. J. Leeper, C. L. Ruiz, G. W. Cooper, K. D. Hahn, J. McKenney, A. C. Owen, G. R. McKee, G. T. Leifeste, D. J. Ampleford, E. M. Waisman, A. Harvey-Thompson, R. J. Kaye, M. H. Hess, S. E. Rosenthal, and M. K. Matzen, IEEE Trans. Plasma Sci. **40**, 3222 (2012).
[2]S. A. Slutz, M. C. Herrmann, R. A. Vesey, A. B. Sefkow, D. B. Sinars, D. C. Rovang, K. J. Peterson, and M. E. Cuneo, Phys. Plasmas **17**, 056303 (2010).
[3]R. D. McBride, M. R. Martin, R. W. Lemke, J. B. Greenly, C. A. Jennings, D. C. Rovang, D. B. Sinars, M. E. Cuneo, M. C. Herrmann, S. A. Slutz, C. W. Nakhleh, D. D. Ryutov, J.-P. Davis, D. G. Flicker, B. E. Blue, K. Tomlinson, D. Schroen, R. M. Stamm, G. E. Smith, J. K. Moore, T. J. Rogers, G. K. Robertson, R. J. Kamm, I. C. Smith, M. Savage, W. A. Stygar, G. A. Rochau, M. Jones, M. R. Lopez, J. L. Porter, and M. K. Matzen, Phys. Plasmas **20**, 056309 (2013).
[4]M. R. Gomez, S. A. Slutz, A. B. Sefkow, D. B. Sinars, K. D. Hahn, S. B. Hansen, E. C. Harding, P. F. Knapp, P. F. Schmit, C. A. Jennings, T. J. Awe, M. Geissel, D. C. Rovang, G. A. Chandler, G. W. Cooper, M. E. Cuneo, A. J. Harvey-Thompson, M. C. Herrmann, M. H. Hess, O. Johns, D. C. Lamppa, M. R. Martin, R. D. McBride, K. J. Peterson, J. L. Porter, G. K. Robertson, G. A. Rochau, C. L. Ruiz, M. E. Savage, I. C. Smith, W. A. Stygar, and R. A. Vesey, Phys. Rev. Lett. **113**, 155003 (2014).
[5]D. B. Sinars, S. A. Slutz, M. C. Herrmann, R. D. McBride, M. E. Cuneo, K. J. Peterson, R. A. Vesey, C. Nakhleh, B. E. Blue, K. Killebrew, D. Schroen, K. Tomlinson, A. D. Edens, M. R. Lopez, I. C. Smith, J. Shores, V. Bigman, G. R. Bennett, B. W. Atherton, M. Savage, W. A. Stygar, G. T. Leifeste, and J. L. Porter, Phys. Rev. Lett. **105**, 185001 (2010).
[6]Y. Y. Lau, J. C. Zier, I. M. Rittersdorf, M. R. Weis, and R. M. Gilgenbach, Phys. Rev. E **83**, 066405 (2011).
[7]J. C. Zier, R. M. Gilgenbach, D. A. Chalenski, Y. Y. Lau, D. M. French, M. R. Gomez, S. G. Patel, I. M. Rittersdorf, A. M. Steiner, M. Weis, P. Zhang, M. Mazarakis, M. E. Cuneo, and M. Lopez, Phys. Plasmas **19**, 032701 (2012).
[8]S. V. Lebedev, D. J. Ampleford, S. N. Bland, S. C. Bott, J. P. Chittenden, J. Goyer, C. Jennings, M. G. Haines, G. N. Hall, D. A. Hammer, J. B. A. Palmer, S. A. Pikuz, T. A. Shelkovenko, and T. Christoudias, Plasma Phys. Controlled Fusion **47**, A91 (2005).
[9]J. D. Douglass, S. A. Pikuz, T. A. Shelkovenko, D. A. Hammer, S. N. Bland, S. C. Bott, and R. D. McBride, Phys. Plasmas **14**, 012704 (2007).
[10]J. L. Giuliani, Jr., F. N. Beg, R. M. Gilgenbach, V. L. Kantsyrev, B. R. Kusse, V. V. Ivanov, and R. Presura, IEEE Trans. Plasma Sci. **40**, 3246 (2012).
[11]J. C. Valenzuela, G. W. Collins IV, D. Mariscal, E. S. Wyndham, and F. N. Beg, Phys. Plasmas **21**, 031208 (2014).
[12]I. Blesener, B. Kusse, K. Blesener, J. Greenly, and D. Hammer, IEEE Trans. Plasma Sci. **40**, 3313–3318 (2012).
[13]V. V. Shlyaptseva, V. L. Kantsyrev, A. S. Safronova, A. A. Esaulov, I. Shrestha, M. E. Weller, G. C. Osborne, and S. F. Keim, Int. J. Mod. Phys.: Conf. Ser. **32**, 1460324 (2014).
[14]G. C. Burdiak, S. V. Lebedev, F. Suzuki-Vidal, G. F. Swadling, S. N. Bland, N. Niasse, L. Suttle, M. Bennet, J. Hare, M. Weinwurm, R. Rodriguez, J. Gil, and G. Espinosa, J. Plasma Phys. **81**, 365810301 (2015).
[15]P. A. Gourdain, R. J. Concepcion, M. T. Evans, J. B. Greenly, D. A. Hammer, C. L. Hoyt, E. Kroupp, B. R. Kusse, Y. Maron, A. S. Novick, S. A. Pikuz, N. Qi, G. Rondeau, E. Rosenberg, P. C. Shrafel, C. E. Seyler, and T. C. Shelkovenko, Nucl. Fusion **53**, 083006 (2013).
[16]K. J. Peterson, D. B. Sinars, E. P. Yu, M. C. Herrmann, M. E. Cuneo, S. A. Slutz1, I. C. Smith, B. W. Atherton, M. D. Knudson, and C. Nakhleh, Phys. Plasmas **19**, 092701 (2012).
[17]P. Zhang, Y. Y. Lau, I. M. Rittersdorf, M. R. Weis, R. M. Gilgenbach, D. Chalenski, and S. Slutz, Phys. Plasmas **19**, 022703 (2012).
[18]M. R. Weis, P. Zhang, Y. Y. Lau, P. F. Schmit, K. J. Peterson, M. Hess, and R. M. Gilgenbach, Phys. Plasmas **22**, 032706 (2015); **21**, 122708 (2014).
[19]A. A. Kim, M. G. Mazarakis, V. A. Sinebryukhov, B. M. Kovalchuk, V. A. Visir, S. N. Volkov, F. Bayol, A. N. Bastrikov, V. G. Durakov, S. V. Frolov, V. M. Alexeenko, D. H. McDaniel, W. E. Fowler, K. LeChien, C. Olson, W. A. Stygar, K. W. Struve, J. Porter, and R. M. Gilgenbach, Phys. Rev. Spec. Top.–Accel. Beams **12**, 050402 (2009).
[20]M. G. Mazarakis, W. E. Fowler, K. L. LeChien, F. W. Long, M. K. Matzen, D. H. McDaniel, R. G. McKee, C. L. Olson, J. L. Porter, S. T. Rogowski, K. W. Struve, W. A. Stygar, J. R. Woodworth, A. A. Kim, V. A. Sinebryukhov, R. M. Gilgenbach, M. R. Gomez, D. M. French, Y. Y. Lau, J. C. Zier, D. M. VanDevalde, R. A. Sharpe, and K. Ward, IEEE Trans. Plasma Sci. **38**, 704 (2010).
[21]See www.goodfellow.com for thin foils of various materials.
[22]S. A. Pikuz, V. M. Romanova, N. V. Baryshnikov, M. Hu, B. R. Kusse, D. B. Sinars, T. A. Shelkovenko, and D. A. Hammer, Rev. Sci. Instrum. **72**, 1098 (2001).
[23]K. J. Peterson, E. P. Yu, D. B. Sinars, M. E. Cuneo, S. A. Slutz, J. M. Koning, M. M. Marinak, C. Nakhleh, and M. C. Herrmann, Phys. Plasmas **20**, 056305 (2013).
[24]T. J. Awe, R. D. McBride, C. A. Jennings, D. C. Lamppa, M. R. Martin, D. C. Rovang, S. A. Slutz, M. E. Cuneo, A. C. Owen, D. B. Sinars, K. Tomlinson, M. R. Gomez, S. B. Hansen, M. C. Herrmann, J. L. McKenney, C. Nakhleh, G. K. Robertson, G. A. Rochau, M. E. Savage, D. G. Schroen, and W. A. Stygar, Phys. Rev. Lett. **111**, 235005 (2013).
[25]S. V. Lebedev, F. N. Beg, S. N. Bland, J. P. Chittenden, A. E. Dangor, M. G. Haines, K. H. Kwek, S. A. Pikuz, and T. A. Shelkovenko, Phys. Plasmas **8**, 3734 (2001).